



Fundamental Understanding of the Synthesis of Well-Defined Supported Non-Noble Metal Intermetallic Compound Nanoparticles

Journal:	<i>Catalysis Science & Technology</i>
Manuscript ID	CY-ART-01-2022-000183.R1
Article Type:	Paper
Date Submitted by the Author:	04-Apr-2022
Complete List of Authors:	Song, Yuanjun; Southeast University, School of Electronic Science and Engineering He, Yang; Oak Ridge National Laboratory, Chemical Science Division Laursen, Siris; University of Tennessee, Chemical Engineering

Cite this: DOI: 00.0000/xxxxxxxxxx

Fundamental Understanding of the Synthesis of Well-Defined Supported Non-Noble Metal Intermetallic Compound Nanoparticles[†]

Yuanjun Song,^a Yang He,^b and Siris Laursen^{*c}

Received Date

Accepted Date

DOI: 00.0000/xxxxxxxxxx

Access to well-defined, model-like, non-noble metal intermetallic compound nanomaterials (<10nm) with phase pure bulk, bulk-like 1st-atomic-layer surface composition, and unique electronic and surface chemical properties is critical for the fields of catalysis, electronics, and sensor development. Non-noble metal intermetallic compounds are compositionally ordered solid compounds composed of transition metals and semimetals or post-transition metals. Their synthesis as model-like high-surface-area supported nanoparticles is challenging due to the elevated reactivity of the constituent elements and their interaction with the support material. In this study, we have developed a systematic understanding of the fundamental phenomena that control the synthesis of these materials such that phase pure bulk nanoparticles (<10nm) may be produced with bulk-like surface terminations. The effect precursor and support choice, chemical potential of H₂, reduction temperature, and annealing procedures were investigated to understand the fundamental kinetics of particle formation and interactions that dictate phase purity and stability and 1st-atomic-layer surface composition. The understanding developed may serve as a foundation for further developing advanced synthesis procedures for well-defined nanoparticles with increasing compositional complexity.

1 Introduction

The science and technology of heterogeneous catalysis is particularly important in the 21st century due to pressing energy and environmental challenges that face society. Catalytic materials play a central role in the production of nearly all fuels and chemicals and in the cleanup of the unwanted side products that pollute the environment.^{1–6} For over a century, the field of catalysis has focused on the development of heterogeneous catalysts such as zeolites, platinum group metals (PGM), and PGM derived PGM+transition metal (TM) alloys.^{7–16} These catalysts have exhibited sufficient, but not necessarily ideal catalytic performance in many foundational industrialized catalytic reactions. However, these classic catalytic materials often struggle to perform new reactions that require markedly different balances of sur-

face chemistry. PGM-based catalysts are also very costly and limit widespread application of catalysis in distributed chemicals and fuels production or use.^{6,17–19} Therefore, the need for new, inexpensive non-noble metal-based catalytic materials that exhibit a much more diverse combination of surface chemistry towards C, O, and H and the bonds that contain them still persists. Of specific contemporary need, are catalysts that exhibit elevated surface reactivity towards oxygen and nitrogen, lower surface reactivity towards unsaturated C=C bonds, limited hydrogenation kinetics, and activity in C–C, C–O, and C–N bond formation reactions.^{15,18,20–35}

In the development of new heterogeneous catalysts, it is known that most pure elements outside of the noble metals exhibit too high of chemical reactivity towards the organic elements (C, O, N, H, etc.) and bonds that contain them to be efficient catalysts at reasonable temperatures (T<600°C).^{18,19,36} However, seminal Ultra-High Vacuum (UHV) surface science studies performed on single crystal materials clearly illustrated that the reactivity of non-noble metals (Mo, W, and V) could be reduced through the formation of TM solid compounds (Mo₂C, Mo₂N, VC, and W₂C) via reaction with p-block elements to produce surface chemistry similar to that of PGMs.^{37–43} Further insight into potential new non-noble metal catalyst formulations was provided by studies that focused upon modification of existing noble (Pd, Pt, Rh, and Ru) and non-noble (Ni, Co, and Fe) metal catalysts

^a Joint International Research Laboratory of Information Display and Visualization, School of Electronic Science and Engineering, Southeast University, Nanjing, 210096, People's Republic of China.

^b Chemical Science Division, Oak Ridge National Laboratory, Oak Ridge, Tennessee 37831, United States.

^c Department of Chemical and Biomolecular Engineering, University of Tennessee, Knoxville, Tennessee 37996, United States. Fax: +1 865 9747076; Tel: +1 865 9745786; E-mail: slaursen@utk.edu

[†] Electronic Supplementary Information (ESI) available: [Additional EDX and XRD characterizations, and a summary table of percentage of NiGa phase after reduction with different H₂ chemical potentials]. See DOI: 00.0000/00000000.

with p-block elements (B, Al, Ge, Sn, Pb, Bi, Sb, Te, and Tl) to tune surface chemistry.^{4,20,22,25,44–51} Later UHV surface science studies focused on the use of larger p-block elements in Pt₃Sn, Pt₂Sn, PtSn, Pd₃Sn, and Pd₂Sn single crystals solidified the presence of unique surface chemistry presented by TM solid compounds.^{4,22,47,52,53} These seminal studies illustrated that surface chemistry could be tuned to be more ideal in many catalytic reactions by the addition of p-block elements and have propelled the community to investigate TM solid compound catalysts. More recent studies have illustrated the utility of many TM solid compound catalysts in a host of classic and contemporary catalytic reactions with a notable focus on TM carbides and phosphides and TMs bound with post transition metals (Pd+Ga, Pd+In, Pd+Sn, Pt+Sn, Ni+Al, Ni+Ga, and Ni+Sn).^{2,21,28,30,32,54–65} However, to systematically study and understand the surface chemistry and fully realize non-noble metal compound catalysts, the community needs high surface area materials that are well defined both in bulk crystal structure (phase) and surface composition. Herein, we focus on fundamental aspects of the synthesis of well-defined/model-like supported high-surface-area binary non-noble TM solid compound nanoparticles composed of one TM element and one post-transition metal element. These atomically ordered TM solid compounds composed of crystalline mixtures of transition metals (TM) and post-transition metals or semimetals (pTM) are intermetallic compounds (IMC), but are also known as ceramics in the materials science community and are distinct from compositionally disordered alloys.

Traditional methods for production of an ingot of material are through arc melting and high-frequency heating methods at high temperature, followed by ball-milling to produce particles with particle size in a scale of micrometers.^{66–77} Despite the ingot method providing phase-pure materials initially, the method offers little control of morphology, particle size, and particle surface composition when producing particles from the ingot through grinding or ball milling.^{66–68} In addition, the particles can be contaminated and oxidized during the milling process due to the use of a solvent. For example, Pd₂Ga synthesized by ball milling showed the formation of gallium oxide over the surface of IM during the ball milling.^{78,79} This issue is often corrected by utilizing a reductive pre-treatment step after particle formation with and without additional annealing procedures. However, the initial oxidation can drive element segregation at the particle surface that may directly affect the particle surface composition even after reductive and annealing procedures.^{58,80}

Low-temperature liquid phase methods such as co-reduction, sol-gel, solvothermal, and hydrothermal synthesis that produce IMC colloids have been developed and employ strong reducing agents to drive precursor reduction and IMC formation.^{81–91} However, this approach can easily lead to kinetically trapped species and mixed-phase materials since the reducing agent cannot provide enough vibrational energy for structural relaxation of IMC crystallites. Likewise, highly reactive reducing and capping agents can strongly influence the particle surface composition and may drive the formation of surface compositions that include elements from the reagents when they are removed at elevated temperatures.

Supported IMC nanoparticles with high surface area are generally much more favorable catalytic materials and have been prepared via incipient wetness impregnation, deposition precipitation, and chemical vapor deposition (CVD) methods.^{3,5,23,54,59,67,92–97} However, many studies have produced multi-phase materials and have either not measured or used less-surface-sensitive techniques such as X-ray photoelectron spectroscopy (XPS) to measure IMC surface composition.^{63,98–101} Nonetheless, some studies, including our investigations, have produced phase-pure materials to illustrate the effect of IMC composition on catalytic performance. For example, using the synthesis understanding presented herein, we prepared SiO₂ and Al₂O₃ supported Ni+Ga IMCs with single pure bulk phase for dehydrogenation of alkane and propane steam reforming reactions.^{28,30,32} Similarly, phase-pure Ni+Ga IMC catalysts have been illustrated in CO₂ partial reduction for the production of small alcohols.^{3,5} Additionally, phase pure Ni₃Sn₂ nanoparticles on Al₂O₃, ZnO, and TiO₂ supports were shown to exhibit higher catalytic activity and improved selectivity in comparison to bulk Ni₃Sn₂ particles in the selective hydrogenation of unsaturated aldehydes for the production of unsaturated alcohols.⁵⁴ In addition, a suite of SiO₂ supported Ni+Sn IMCs with pure bulk phase (Ni₃Sn, Ni₃Sn₂ and Ni₃Sn₄) were prepared by using CVD method.⁶⁷ These studies illustrate that phase-pure supported IMC nanoparticle catalysts can be produced and the need for phase purity.

Beyond bulk phase purity, IMC particle surface composition must be similarly controlled and measured using appropriately surface sensitive techniques (e.g., 1st atomic layer). Because of the general lack of truly surface sensitive characterization techniques, the dominant portion of prior studies have utilized techniques that yield information from the topmost several nanometers of the material (Energy-dispersive X-ray spectroscopy (EDS) line scans and XPS) convoluting connections between surface composition and catalytic performance.^{54,61,67,86,94,102–107} XPS has been employed routinely for many decades to study the elemental surface composition of solids and can be made to be more surface sensitive by tracking core electrons in the energy range of 50–250 eV, but still samples electrons from 1–5nm into the material surface.^{108–110} On the other hand, ablation or ion scattering methods, such time-of-flight secondary ion mass spectrometry (TOF-SIMS) and low or medium energy ion scattering (LEIS and MEIS), are more appropriate to yield more exact surface composition measurements.^{111–116} Despite TOF-SIMS providing compositional information for the first few atomic layers through the formation of free clusters produced by ablation/sputtering, the stability of the clusters can affect the suggested composition of the material surface.^{114–117} On the other hand, ion scattering techniques allow for the measurement of the true 1st atomic layer surface composition. With a recent improvement in detector technology, the sensitivity of the LEIS technique has been dramatically improved and recoincided as high-sensitivity LEIS (HS-LEIS) and is becoming more available to the community.^{112,113,118–123} In the design of catalytic or sensing materials, it is vital to produce materials with measured and controlled 1st atomic layer compositions such that clear connections between surface composition and ma-

terial performance may be developed.

Herein, we present many years of work that have focused upon understanding critical fundamental aspects of the synthesis of well-defined/model-like high surface area supported nanoparticle late non-noble TM IMCs. Again, we define "well-defined/model-like" materials as materials that exhibit a single crystal phase and bulk-like surface compositions. This report outlines understanding developed through the synthesis of Ni+Ga, Ni+In, and Co+Ga IMCs. Our studies focused upon understanding the effects of precursor reduction kinetics, choice of inorganic precursor, H₂ chemical potential and temperature during reduction on the formation of the IMCs and the role of extended annealing environments on particle growth and particle surface composition. The effect of support surface chemistry in the formation of the IMCs was also investigated. These studies have shed light upon the fundamental kinetics of precursor reduction, element diffusion across the support, and the formation of IMCs. It should be noted that the techniques developed in this study should enable the production of late TM IMCs when both TM and p-element precursors can be reduced at temperatures below 800°C under pure H₂. Synthesis of IMCs composed of more reactive earlier TMs or p-elements will likely require higher energy techniques and/or organic precursors. Nonetheless, the understanding developed has paved the way for the community to access a large suite of model-like materials such that clear connections between surface chemistry and catalytic performance may be developed.

2 Method

2.1 Experimental Method

2.1.1 Synthesis of Supported Intermetallic Compounds

SiO₂ and partially oxidized carbon supported Ni+Ga IMC catalysts with 3:1, 5:3, 1:1, and 2:3 nominal loadings (10wt%) were synthesized via incipient wetness impregnation method. A defined amount of Ni(NO₃)₂·6H₂O (Sigma Aldrich) and Ga(NO₃)₃·xH₂O (Sigma Aldrich) metal precursors were deposited on SiO₂ (Alfa Aesar, amorphous fumed, 350-420 m²/g)^{124,125} or partially oxidized carbon. Partially oxidized carbon was homemade via oxidation of BLACK PEARLS® 2000 carbon black from CABOT corporation (1200-1500 m²/g, 15nm) in boiling 70% nitric acid solution with a reflux setup for 2 hrs, and the potential surface oxygen groups include CO- and CO₂-evolving carboxylic groups (such as C–OH, C–O–C, C=O and C–OOH).^{126–128} Ga(NO₃)₃ was first dissolved in a small amount of 30wt% nitric acid solution at 70°C, then Ni(NO₃)₂ was added. After both precursors were completely dissolved, the mixture was deposited on support. It is worth noting that inappropriate deposition procedures may produce inhomogeneous distributions of constituent elements on the support surface leading to multi-phase IMCs.^{129,130} Thus, the paste needs to be continually stirred for around 20 mins till homogeneous and evaporative-transport of salts to evaporation fronts is limited. Then, all samples were dried at 100°C under Ar flow for 12 hrs.

Al₂O₃ (Alfa Aesar, 70% delta and 30% gamma, 50-100 nm)^{28,30} supported 1:1 Ni:Ga IMCs (10wt%) was synthesized via hydroxide method using Ni(NO₃)₂·6H₂O (Sigma Aldrich)

and Ga(NO₃)₃·xH₂O (Sigma Aldrich) metal precursors. A defined amount of Ga(NO₃)₃·xH₂O was first dissolved into 150 mL D.I. water at 70°C. Then pH value was adjusted to 3.9 using diluted NaOH solution to transform the Ga precursor into a hydroxy-nitrate. Support was then added to the solution and aged for 0.5 hr. Next, a specific amount of Ni(NO₃)₂·6H₂O (1:1 Ni:Ga nominal loading) was introduced and transformed into the hydroxy-nitrate form at the pH of 7.0. The solution was aged for another 0.5 hr. The sample was then washed, filtered, and then dried under air at 100°C for 3 hrs. SiO₂ supported Ni+In (Ni₂In₃ and Ni₂In) IMCs were also synthesized using same hydroxide method except for transforming In(NO₃)₃·xH₂O to hydroxy-nitrate species at pH=3.

As-reduced samples were pretreated under pure H₂ at 700°C for 2 hrs, and the effect of H₂ chemical potential (from 2% to 100%) and reduction temperature (400~700°C) on bulk composition, crystal phase distribution, and particle surface composition were investigated. Two types of annealing pretreatment including direct-annealing and freeze-annealing were performed. With direct-annealing, samples were annealed under 2% H₂ in Ar or pure Ar at 700°C for 12 hrs directly after reduction without cooling treatment. On the other hand, freeze-annealing allowed particles to cool down to room temperature under H₂ to fully crystallize and then heated again to 700°C under 2% H₂ for 12 hrs for annealing. Direct-annealed Ni₃Ga/SiO₂ was prepared via direct-annealing at 700°C under 2% H₂ in Ar for 12 hrs directly after reduction of 3:1 Ni:Ga/SiO₂ under 100% H₂ at 700°C for 2 hrs. Freeze-annealed samples were produced via freeze-annealing at 700°C under 2% H₂ in Ar for 12 hrs after the reduction at 700°C under 100% H₂ with cooling down to room temperature. To be clear, the temperature of the gas switch from 100% H₂ to 2% H₂ in direct-annealing was at 700°C, while freeze-annealing was at room temperature.

2.1.2 Characterizations

X-ray powder diffraction (XRD) on PANalytical X'Pert Pro system using Cu Kα radiation (ORNL) was performed to identify the bulk phase and crystal structure of particles. Long acquisition time of a minimum of 3 hrs was used to improve the detection of minority phases (2θ range is from 10 to 90° and the step size is 0.017° with 0.006°/s scanning rate). To obtain more details of crystal structure of materials, high-resolution XRD with synchrotron radiation was performed at the beamline 11-BM at the Advanced Photon Source (APS) with mail-in service in Argonne National Laboratory, which uses an average wavelength of 0.41 with a step size of 0.001° and scan speed of 0.01°/s and 2θ range 0.5-50°. With respect to the characterization of surface composition, high-sensitivity low energy ion scattering (HS-LEIS) spectroscopy with an IONTOF Qtac100 spectrometer (Lehigh University) was used. LEIS samples were prepared in our lab. After cooling down to room temperature, they were passivated under 2% O₂/Ar atmosphere for 1 hour which is the normal procedure used in the community to protect more reactive samples from autocatalytic oxidation. The samples were then transferred to a sealed sample tube filled with nitrogen. Before LEIS measurement, samples were introduced to the UHV chamber and exposed to room temperature

low-energy neutral H atoms for 30 mins to remove any oxidation layer. Both a surface survey scan and depth profiling were performed using 5keV Ne⁺ ions. In a surface survey scan, to seek targeted elements with better signal-to-noise ratio, an ion dose of $5 \times 10^{14} \text{ cm}^{-2}$ with a wide energy range was used. In depth profiling, a sputter beam of 0.5 keV Ar⁺ with 1×10^{14} ions cm^{-2} was used for removal of approximately 0.1 nm atomic layer per cycle so that the ratio of integrated scattering intensity of probe elements (such as Ni-to-Ga) in each layer can be tracked and normalized to the bulk stoichiometry for the estimation of elemental composition at other layers. In this work, the depth profiling of SiO₂ supported Ni₃Ga and CoGa were performed to utilize as the normalized references for the analysis of surface compositions of Ni+Ga and Co+Ga IMCs. Particle morphology, size, and size distribution were characterized utilizing transmission electron microscopy (TEM) and high-resolution energy-dispersive X-Ray spectroscopy (HR-EDS). Samples were prepared by dispersing sample powder in methanol and sonicated before being deposited on the TEM grids. TEM measurements on all of the samples were performed on ZEISS LIBRA 120 operating at 120 KV at University of Tennessee, Knoxville. STEM HAADF and HR-EDS measurements were performed on Talos FEI F200X operating at 200 KV at Oak Ridge National Lab (ORNL).

3 Results and Discussion

3.1 Effect of Salt Choice on Reduction Dynamics

Studies first focused upon understanding the kinetics of inorganic precursor reduction using temperature-programmed reduction (TPR) by H₂ with the expectation that complete co-reduction of TM and p-element precursors was needed to promote the formation of phase pure IMC nanoparticles with stoichiometry that equalled that of nominal loadings. The TPR of Ni, Ga, and In nitrate, chloride, and hydroxide precursor salts deposited on Al₂O₃ and SiO₂, alone and combined, was investigated in the context of forming Ni+Ga and Ni+In IMC nanoparticles (Figure 1). In the individual TPR of the inorganic Ni and Ga nitrate, chloride, and hydroxide or In nitrate and hydroxide precursors, nitrate precursors exhibited more complete reduction at lower temperatures. The Ni and Ga chloride precursors required higher temperature for complete reduction and likely left chlorine at the metal-support interface.^{131–134} All hydroxide precursors exhibited significant support-induced stabilization, which resulted in inhomogeneous reduction dynamics (bi- or multi-modal) and the need for higher temperatures for complete reduction.^{135–137} The effect of support-induced stabilization and spillover of dissociated H₂ have been investigated and understood by many others previously in the synthesis of oxide-supported metal catalysts.^{138–140} In co-deposition TPR studies, most of the same dynamics were observed, yet the presence of Ni helped to promote the reduction of p-element precursors likely via an atomic H spillover effect.^{141,142} However, in the co-deposition of Ni and Ga or In hydroxides, support-induced stabilization resulted in even more pronounced inhomogeneous/multi-modal reduction dynamics. The effect of support choice, SiO₂ vs. Al₂O₃, was investigated for In(NO₃)₃ alone and co-deposited Ni(NO₃)₂ and In(NO₃)₃. Results indi-

cated that In(NO₃)₃ was stabilized more over Al₂O₃ vs. SiO₂ resulting in more significant inhomogeneous reduction dynamics. However, when co-deposited with Ni(NO₃)₂, reduction was dramatically improved over both supports with complete reduction achieved below 450°C. Results agree well with prior studies that investigated the TPR of various Ni inorganic salts.^{132,143–145} In general, results indicated that nitrate salts would likely be most ideal to achieve complete reduction of both TM and p-element precursors at relatively low temperatures. Additionally, utilizing supports with low surface reactivity like SiO₂ can aid in ensuring complete reduction of precursors. A similar conclusion was derived in a study focused on producing Pd-based IMCs with Bi, Sn, and Pb where PdBi/Al₂O₃ with pure phase could be produced, yet Pd₃Sn and Pd₃Pb exhibited multi-phase compositions likely due to large differences in reduction kinetics of Pd, Sn, and Pb salts.⁹⁶

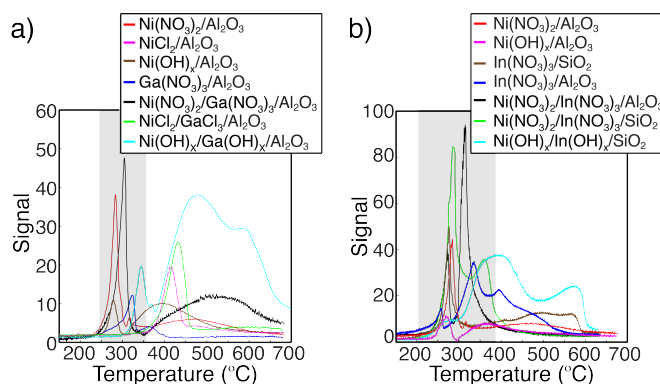


Fig. 1 Temperature programmed reduction (TPR) of Al₂O₃- and SiO₂-supported Ni, Ga, and In inorganic precursors (nitrate, chloride, or hydroxide) deposited alone or in binary couples (Ni+Ga or Ni+In). A weight loading of 10 wt% of each precursor was utilized. The reducing environment was 5% H₂ in Ar.

It is useful to note that when extending these results to other precursors, one must be cognizant of and avoid the unfavorable formation of hydroxides or oxides during deposition when employing H₂O. For example, the In(NO₃)₃ precursor can react with H₂O to form complexes that contain hydroxide ligands that will stabilize the complex when in contact with certain supports and inhibit complete reduction.¹⁴⁶ One approach to avoid the formation of In(OH)_x(NO₃)_x was to add a small amount of nitric acid to the slurry during deposition. In the synthesis of Ge-based IMCs, this issue is far more pronounced with GeO₂ formation occurring if aqueous deposition is attempted. Therefore, it may be necessary to utilize organometallic precursors in a water/air-free environment to produce IMCs from more reactive elements, e.g., earlier TMs and later p-elements. For example, Komatsu and coworkers showed that phase pure Ni₃Ge could be produced inside the mesopores of MCM-41 through the formation of reduced Ni species followed by CVD of Ge(CH₃)₄ with H₂.⁵⁹ Likewise, the formation of phase pure IMCs of Mo, Ta, and Nb has only been achieved via the melt method or physical vapor deposition because of the stability of their inorganic salts and high oxophilicity leading to slow reduction kinetics.^{71,73,74,147} In the end, production of IMCs composed of late-TMs and early and larger p-

elements that are both easier to reduce when present as inorganic salts will likely be more facile. Whereas, production of IMCs composed of mid to early TMs or smaller or later p-elements may require new energy delivery techniques like light- or microwave-assisted reduction when using inorganic precursor salts or the use of organometallic precursors in water/air-free environments.

3.2 Effect of Reduction Temperature and Support Surface Chemistry

After identifying precursors and conditions that allow for more complete reduction of precursors, we aimed to understand the effect of support surface chemistry on the formation of nanoparticle IMCs. We investigated the formation of Ni+Ga IMCs on fumed silica, partially oxidized carbon, and Al₂O₃ (70% delta, and 30% gamma) supports under 100% H₂ as a function of temperature. Ni+In IMC formation was only studied using the SiO₂ support. Nitrite precursors were deposited via incipient wetness and reduced using a minimum reduction temperature of 400°C under 100% H₂ to ensure complete precursor reduction and limit any effects associated with limited H₂ chemical potential. Nominal loadings of 1:1 TM and p-elements were employed with the expectation that off-nominal TM-rich or lean stoichiometries could be produced if element diffusion or IMC kinetics were limited at the temperature employed. In the absence of kinetic limitations along the synthesis mechanism, production of the 1:1 phases of IMCs was expected, namely NiGa and NiIn. Long-acquisition time pXRD (3.5 hrs) was utilized to analyze the IMC phases produced (see Figure 2a-d). The surface reactivity of the supports is expected to increase in the order of partially oxidized carbon < SiO₂ < Al₂O₃ and influence reduced element diffusion kinetics.

In the case of Ni+Ga IMC formation, a clear effect of support surface chemistry in dictating reduced element diffusion and IMC phase evolution was observed. The stability of the Ni+Ga IMC phases can be estimated from the phase diagram using melting points and is ordered from most to least stable as Ni₃Ga > Ni₅Ga₃ > NiGa.¹⁴⁸ The order of phase stability would also suggest the kinetics of formation of each phase if a BEP-like correlation between thermodynamics and kinetics exists. Indeed, Ni+Ga IMC synthesis using SiO₂ as a support illustrated that Ni₃Ga was the most kinetically preferred phase, as it formed readily in phase-pure form at 400°C. As reduction temperature increased to 500°C, the next most stable phase of Ni₅Ga₃ dominated the sample with a minority of Ni₃Ga persisting. At 700°C, the NiGa phase could be produced in pure form. These results suggested that the chemical potential of Ni and Ga provided by the nominal loading was not sufficient to overcome kinetic limitations associated with reduced element diffusion at lower temperatures. However, it could dictate the IMC phase if appropriate vibrational energy was supplied. Utilizing a support with lower surface reactivity, namely partially oxidized carbon, the BEP-like correlation was still followed and phase pure Ni₃Ga could be produced at 400°C, while pure phase Ni₅Ga₃ was produced at 500°C and NiGa at 700°C. Since the total metal loading was the same over SiO₂ vs carbon supports, the width at half maximum of the pXRD reflections suggested

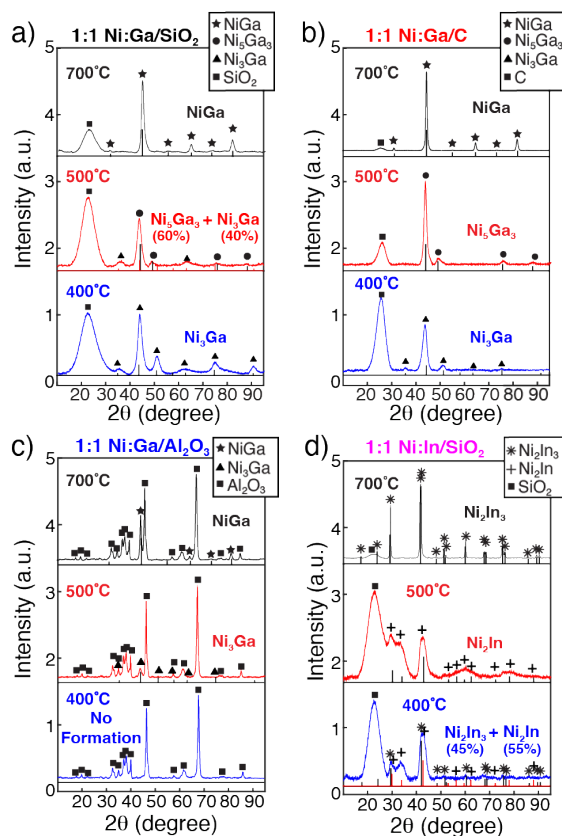


Fig. 2 Long-acquisition-time pXRD of a) 1:1 Ni:Ga/SiO₂, b) 1:1 Ni:Ga/C, c) 1:1 Ni:Ga/Al₂O₃, and d) 1:1 Ni:In/SiO₂ after reduction with pure H₂ at 400°C, 500°C, and 700°C.

larger well-crystallized particles were produced over the carbon support further suggesting improved reduced element diffusion as support surface reactivity was reduced. Utilizing a support with elevated surface reactivity, namely Al₂O₃ (70% delta, and 30% gamma), significantly limited diffusion of the constituent elements inhibited the formation of Ni+Ga IMC at 400°C. As the reduction temperature increased to 500°C, the most kinetically preferred phase of Ni₃Ga was observed, which further confirms the effect of element availability on the IMC phase formed. At 700°C, diffusion kinetics could be surmounted and the formation of NiGa could be achieved once again. Studies of Ni+In IMC formation over SiO₂ suggested that this phenomenon was general since a mixture of Ni₂In and Ni₂In₃ was produced at 400°C, pure Ni₂In was produced at 500°C, and Ni₂In₃ was produced at 700°C, which agrees with the predicted stability of the Ni+In IMC phases in the studies of others.^{60,149,150} A similar phenomenon was also encountered in the studies of Furukawa and Komatsu groups in the production of Pd₃Pb over SiO₂ and Al₂O₃ where phase pure Pd₃Pb could be achieved over SiO₂ and not over Al₂O₃ using the same reduction conditions (pure H₂ at 400°C).^{96,151} It is also useful to note that the strength of bonding between the constituent elements of the IMC and the support are species specific and the late TM elements will be less strongly bound than the more reactive p-elements. This phenomenon likely also dictates the IMC phases observed in this study and will become more prominent

when more reactive constituent elements are employed. In the end, results suggested that utilizing supports with low surface reactivity towards the reduced elements of the IMC favorably promotes the formation of IMC phases that agree with nominal loadings. Therefore, support choice is critical in the production of well-defined supported IMC nanoparticle synthesis.

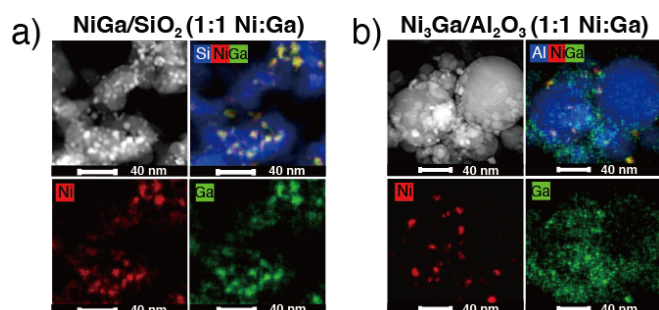


Fig. 3 EDX-mapping of a) NiGa (1:1 Ni:Ga nominal loading) over SiO_2 , which was reduced at 700°C with 100% H_2 for 2 hrs, and b) Ni_3Ga (1:1 Ni:Ga nominal loading) over Al_2O_3 , which was reduced at 500°C with 2% H_2 for 2 hrs, then annealed at 700°C with pure Ar for 12 hrs. Element color code is: Ni (red), Ga (green), and Si or Al (blue)

EDX elemental mapping in STEM of Ni+Ga IMC with 1:1 Ni:Ga nominal loading formation over and SiO_2 and Al_2O_3 (see Figure 3) further confirmed the effect of temperature and support surface chemistry on element diffusion across the support surface. At a reduction temperature of 700°C over SiO_2 , the spatial distribution of Ni and Ga on SiO_2 indicated well-dispersed elements. The same phenomena were observed in the cases of $\text{Ni}_3\text{Ga}/\text{SiO}_2$ and $\text{Ni}_5\text{Ga}_3/\text{SiO}_2$ (see Figure S1). On the other hand, at 500°C over Al_2O_3 , Ni elements are observed collecting in particles, yet portions of the Ga loaded appear to remain dispersed across the support and not incorporated in the IMC particles formed. These results illustrate the difference in Ni vs. Ga diffusion and that Ga diffusion appears to limit the formation of an IMC phase that equals that of the nominal loading. As the p-element binds more strongly to the support, this trend is expected in the case of Ni-based IMCs.

3.3 Effect of H_2 Chemical Potential

To understand if there was an effect of H_2 chemical potential on element diffusion and IMC nanoparticle formation, we utilized Ni+Ga on fumed partially oxidized carbon, silica, and alumina supports deposited using nitrate salts at a loading of 1:1, reduced under at 700°C under a range of H_2 concentrations (from 2% to 100%), and tracked the evolution of the IMC phases via p-XRD (Figure 4). The percentage of target IMC phase (NiGa) was summarized as a function of H_2 chemical potential in the supporting information document (see Table S1). The reduction temperature of 700°C was motivated by prior results that showed IMC phase formation that equaled nominal loading under 100% H_2 . Gas phase flow conditions ensured that the availability of hydrogen was not limiting even at 2% H_2 .

Results showed that the chemical potential of H_2 directly affected element diffusion and correlated well with the expected

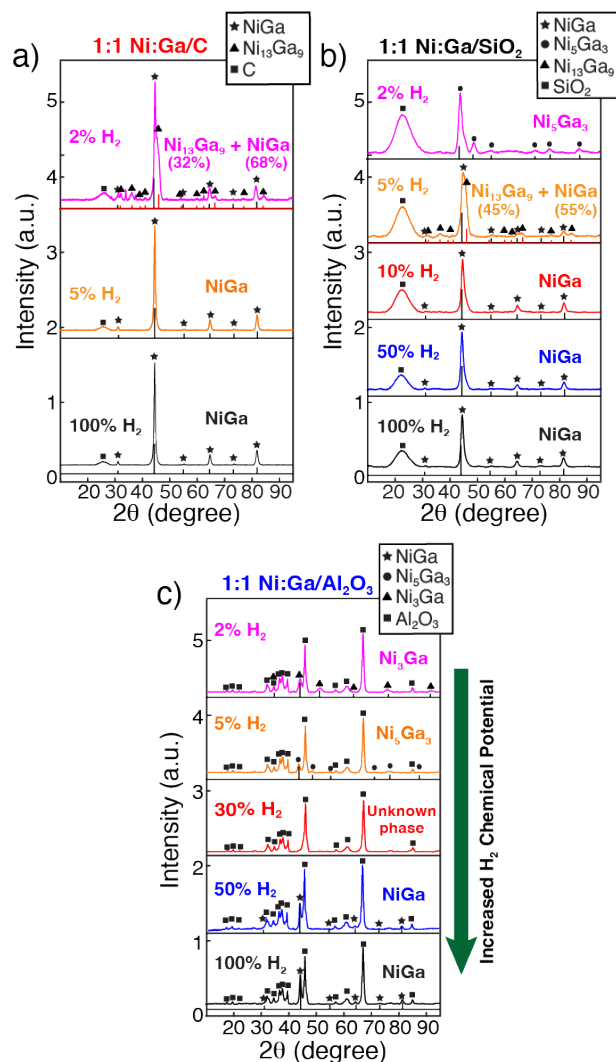


Fig. 4 Long-acquisition-time pXRD of c) 1:1 Ni:Ga/ C , b) 1:1 Ni:Ga/ SiO_2 , and c) 1:1 Ni:Ga/ Al_2O_3 after reduction with different concentrations of H_2 in Ar at 700°C , which illustrated the effect of H_2 chemical potential on bulk composition.

stability of reduced elements on the supports employed (partially oxidized carbon, SiO_2 , and Al_2O_3) indicating a destabilizing effect of atomic H adatoms. Starting with the least reactive support, partially oxidized carbon, NiGa was achieved at a H_2 concentration of 5%, with a mixture of Ni_3Ga and NiGa observed under 2% H_2 . On the other hand, over SiO_2 , 10% H_2 was needed to achieve pure NiGa, with mixtures of Ni_5Ga_3 , Ni_3Ga , and NiGa observed at lower H_2 concentrations. Over the most reactive support utilized, Al_2O_3 , an H_2 concentration of 50% was necessary to achieve phase pure NiGa. At lower H_2 concentrations, the IMC phases of Ni_5Ga_3 and Ni_3Ga were observed on Al_2O_3 , sequentially. Observations suggest that atomic H adatoms either on the support or directly attached to the reduced constituent elements promote their diffusion across the surface of the support. If H_2 chemical potential is not sufficient, diffusion of constituent elements and their chemical potential with respect to IMC nanoparticle growth will be reduced. The effect is most pronounced again for the more reactive p-element, Ga, as evident by Ni-rich IMC

compositions when diffusion is limited. The exact mechanism of the promotion of element diffusion cannot be derived from these studies, but it is reasonable to suggest that bonds between H and reduced elements weaken bonds to the support surface and promote diffusion. It is less likely that the support surfaces become covered by H adatoms and limit the interaction between constituent elements and surface lattice elements. Further investigations are needed to fully understand the fundamental mechanism of this promotion. It is also reasonable to generalize these results and suggest that as constituent element reactivity increases, e.g., early TMs or lighter p-elements, elevated chemical potentials of H₂ will be required to facilitate phase pure IMC nanoparticle formation. Utilizing supports with low surface reactivity would also be beneficial.

Using the understanding developed, we were able to synthesize suits of supported non-noble-metal IMC nanoparticles with pure phase (as shown in Figure S2), including Ni+Ga (Ni₃Ga, Ni₅Ga₃, NiGa, Ni₂Ga₃), CoGa, and Ni+In IMCs (Ni₂In and Ni₂In₃). In addition, the particle size of the phase pure IMCs could be manipulated through an annealing pretreatment, as shown in Figure 5. IMC particle size of as-reduced IMCs was generally around 2-5 nm and could be increased to 4-8 nm after 12 hrs annealing at 700°C under Ar or 2% H₂ in Ar.

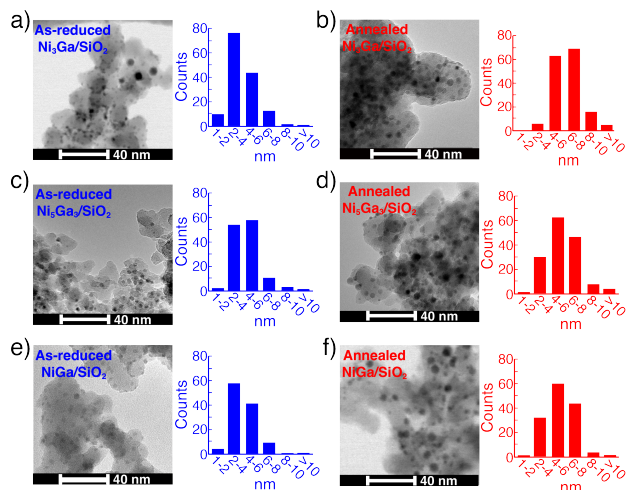


Fig. 5 Electron micrographs and size distributions of as-reduced and annealed SiO₂-supported Ni+Ga IMCs: a) as-reduced Ni₃Ga/SiO₂; b) direct-annealed Ni₃Ga/SiO₂; c) as-reduced Ni₅Ga₃/SiO₂; d) freeze-annealed Ni₅Ga₃/SiO₂; e) as-reduced NiGa/SiO₂; f) freeze-annealed NiGa/SiO₂. Minor particle size growth after 12hrs at 700°C illustrates the stability of the IMC nanoparticles.

3.4 Fundamental Setup for Particle Size Growth and Surface Termination Adjustment

Upon achieving phase pure IMC nanoparticle synthesis, we then focused upon developing annealing procedures to grow IMC particle size to improve bulk phase stability and to adjust particle surface composition to bulk-like where needed. The compositional and structural stabilities of IMCs are crucial if they are to be employed as catalysts, sensors, or electronic components that may encounter reactive gas phase environments at elevated

temperatures or applied potentials. The performance of the supported IMC nanoparticles in catalytic, electronic, or sensing applications is affected by or directly dependent upon the compositional stability of the particle bulk,^{19,21,152–155} surface composition,^{64,80,156–159} and morphology of the particle.^{91,160–162} Control of particle surface composition is also paramount in heterogeneous catalysis and sensing applications. Because the as-reduced Ni+Ga, CoGa, and Ni+In IMC nanoparticles exhibited average particle size distributions around 2-5 nm, their bulk and surface composition stability may be less than ideal for applications that involve elevated temperatures (T>250°C) and contact with reactive chemical environments due to the nano-size effect. Moreover, the reactive environment used to form the IMC nanoparticles may result in element segregation to the particle surface.

Before discussing insights derived from developing annealing procedures, we review the observed IMC particle surface composition of the as-reduced IMCs synthesized. HS-LEIS was utilized to characterize IMC particle surface composition. HS-LEIS is a highly surface sensitive ion scattering technique that provides compositional information of the outermost 1st atomic layer of materials. The probe ion beam was rastered across the sample to minimize ion ablation effects, which are already fairly minimal and do not affect the dominant portion of ions that successfully scatter from the crystal surfaces.

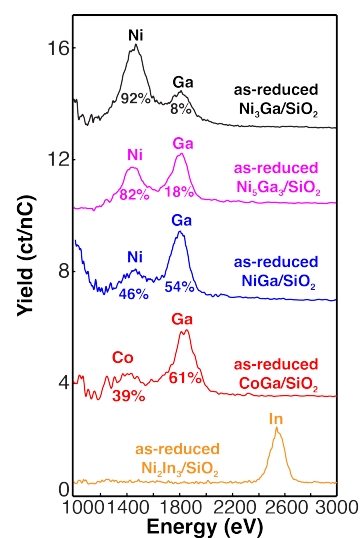


Fig. 6 First atomic layer surface composition characterization of as-reduced SiO₂ supported Ni₃Ga, Ni₅Ga₃, NiGa, CoGa, and Ni₂In₃ IMCs via HS-LEIS.

HS-LEIS characterization of the as-reduced Ni₃Ga, Ni₅Ga₃, NiGa, CoGa, and Ni₂In₃ IMCs indicate that either the TM or the p-element could segregate to the particle surface under the preparation condition (see Figure 6). In the case of as-reduced Ni+Ga IMCs, Ni₃Ga exhibited a Ni-rich surface (92% Ni) while Ni₅Ga₃ and NiGa exhibited a surface composition close to that of the bulk (82% Ni and 46% Ni, respectively). On the other hand, as-reduced CoGa and Ni₂In₃ exhibited slightly Ga-rich (39% Co) and In-dominated (nearly 100% In) surface compositions. Results show a rich energetic phase space determines the as-reduced

IMC particle surface composition. For example, the more stable IMCs of Ni_3Ga , Ni_5Ga_3 , NiGa , and CoGa promote TM-rich or near-bulk-like surface compositions. On the other hand, less stable IMCs composed of p-elements that present inordinately low pure-element surface energies, as in Ni_2In_3 , resulted in p-element-dominated nanoparticle surface compositions. Comparing Ni_3Ga , Ni_5Ga_3 , NiGa , and CoGa further suggested that the chemical potential of the elements within the IMC bulk, as dictated by the TM-to-p-element ratio, plays an energetically-similar role as the innate bulk IMC stability in determining IMC particle surface composition. This is evidenced by both NiGa and CoGa exhibiting more bulk-like surface terminations.

3.5 Effect of Direct and Freeze-Annealing on Phase Disproportionation

Two annealing approaches were investigated to grow particle size and adjust particle surface composition: “direct-annealing” and “freeze-annealing”. In direct-annealing, the as-reduced IMC was subjected to 12 hrs thermal treatment at the original 700°C under a modified gas phase (2% H_2 in Ar or pure Ar) or under pure H_2 without intermediate cooling. In freeze-annealing, the as-reduced IMC was allowed to cool slowly to room temperature under H_2 then reheated to annealing conditions (700°C for 12 hrs under 2% H_2 in Ar). A successful annealing procedure would result in the retention of the as-prepared IMC bulk crystal phase and a particle surface composition near that of the bulk stoichiometry. To clarify, annealing under 2% H_2 in Ar is different from a longer reduction treatment since the phase-pure IMC nanoparticles have already formed. In addition, as Figure 4 illustrates, 2% H_2 in Ar is insufficient to promote the formation of pure bulk phase that agrees with the nominal loading.

First focusing on the bulk crystal phase stability, we investigated the effect of direct-annealing samples under Ar at 700°C for 12 hrs (see Figure 7a). It was found that the procedure induced phase disproportionation of all as-reduced Ni+Ga/SiO_2 IMCs. The bulk phases of $\text{Ni}_3\text{Ga/SiO}_2$, $\text{Ni}_5\text{Ga}_3/\text{SiO}_2$, and NiGa/SiO_2 disproportionated to a mixture of $\text{Ni}_3\text{Ga+Ni+NiO}$, Ni_3Ga , and a mixture of $\text{Ni}_3\text{Ga+Ga}_2\text{O}_3$, respectively (Figure 7a). The source of oxygen for formation of NiO and Ga_2O_3 is likely from SiO_2 support or the nitrates, which also has been observed in studies by other investigators.^{163–166} When 2% H_2 in Ar was utilized during direct-annealing instead of pure Ar, disproportionation in the Ni_3Ga was avoided, yet still occurred for the less stable phases of Ni_5Ga_3 and NiGa (Figure 7b). When utilizing pure H_2 during direct-annealing, phase disproportionation was avoided in all Ni+Ga IMC cases (Figure 7c). Phase disproportionation driven by direct-annealing treatment was also found to be support-dependent and that supports with lower surface reactivity would limit constituent element spill over and phase disproportionation. For example, when utilizing a support with lower surface reactivity, e.g. partially oxidized carbon, the phase purity of NiGa could be retained after direct-annealing under pure Ar and 2% H_2 in Ar (see Figure 7d).

These results suggested that the stability of the IMC nanoparticles directly after their formation at 700°C was dependent upon

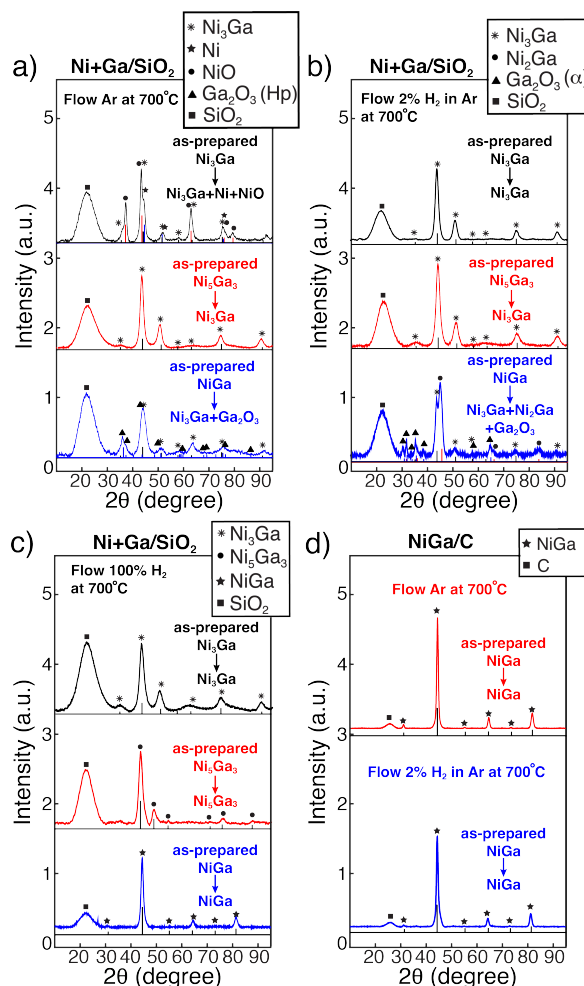


Fig. 7 The effect of direct-annealing as a function of gas phase H_2 concentration and support on IMC initial phase stability: a) as-prepared Ni+Ga/SiO_2 at 700°C under pure Ar; b) as-prepared Ni+Ga/SiO_2 at 700°C under 2% H_2 in Ar; c) as-prepared Ni+Ga/SiO_2 at 700°C under 100% H_2 ; and d) as-prepared NiGa/C at 700°C under pure Ar and 2% H_2 in Ar.

the presence of atomic H adsorbates. It is proposed that strong interactions between constituent elements and the support surface may drive a spill-over-like effect that drives constituent elements back onto the support promoting disproportionation when atomic H adsorbates were absent. In the presence of atomic H adsorbates, elements that spill over onto the support may be destabilized via the same mechanism observed in the initial reductive treatment to form the IMCs. This mechanism appears to promote constituent elements to remain in the IMC particle. Despite this favorable effect, using high H_2 chemical potentials during annealing may lead to element segregation to the IMC particle surfaces because of strong H-element interaction. Therefore, alternate annealing procedures that avoid or minimize the need for H_2 in the gas phase were investigated.

The freeze-annealing procedure was developed through systematic investigation of the effect of direct-annealing temperature on phase disproportionation of SiO_2 supported as-reduced NiGa IMC and revealed that allowing particles to fully crystallize by

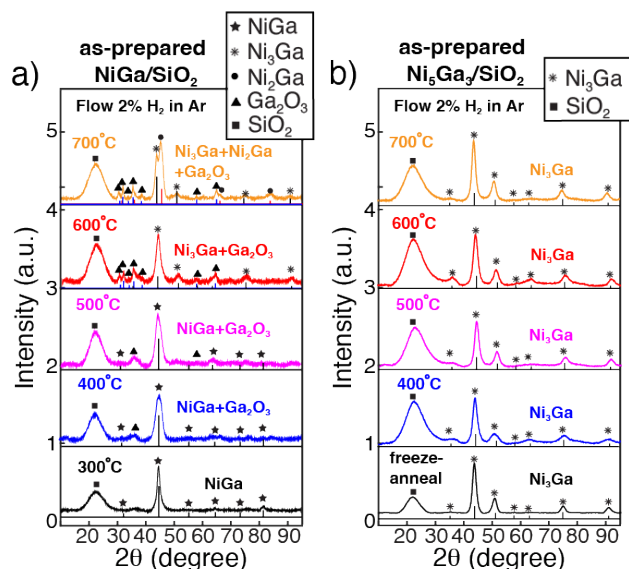


Fig. 8 Effect of direct-annealing temperature on IMC phase stability: a) direct-annealing of as-prepared NiGa/SiO₂ at 300–700°C under 2% H₂ in Ar; b) direct-annealing of as-prepared Ni₅Ga₃/SiO₂ at 400–700°C and freeze-annealing at 700°C under 2% H₂ in Ar.

cooling samples to room temperature under H₂ after initial reduction could aid in avoiding phase disproportionation. As shown in Figure 8a, with direct-annealing at 700°C, SiO₂-supported NiGa was completely transformed to a mixture of Ni₃Ga, Ni₂Ga, and Ga₂O₃ as a result of the spill-over effect. Similarly, at 600°C, NiGa transformed to the mixture of Ni₃Ga and Ga₂O₃. However, when the direct-annealing temperature decreased to 500°C and 400°C, NiGa phase could be maintained but still coexisted with Ga₂O₃. Once the temperature was reduced to 300°C, pure NiGa could be retained.

Shifting to allow the as-prepared IMCs to cool to room temperature under H₂ to allow them to fully crystallize before increasing temperature back up to 700°C for annealing allowed a lower concentration of 2% H₂ to be utilized during annealing. Using this approach, IMC particles of Ni₃Ga, NiGa, CoGa, and Ni₂In₃ remained phase pure after freeze-annealing and enabled the growth of IMC particle sizes from 2–5 nm to 4–8 nm (see Figure 9 and Figure 5). In the case of Ni₅Ga₃, disproportionation was observed even using the freeze-annealing procedure using 2% H₂ in Ar (see Figure 8b). These results indicate that relative stability of the IMC and support surface chemistry towards the constituent elements play a role in IMC stability under annealing conditions and that atomic H adsorbates can counteract spillover effects that lead to phase disproportionation.

3.6 Annealing to Adjust Particle Surface Composition

Returning to focus upon IMC particle surface composition, the direct- and freeze-annealing procedure developed were able to adjust particle surface composition to bulk-like in the cases of Ni₃Ga, NiGa, and CoGa while retaining the initial phase purity of the IMCs (see Figure 9a and 9b). This phenomenon was previously encountered by others in studies where bulk phases of

Pt+Ga were maintained under annealing pretreatment and control of surface termination was achieved via annealing at different temperatures in spite of using less surface sensitive XPS.^{167,168} Ni₂In₃ was the only case where annealing procedures could grow particle size and retain initial phase purity, but not adjust the In-rich surface composition back to bulk-like (see Figure 9c). Fundamentally, results further underscore that the innate stability and relative chemical potential of constituent elements as dictated by bulk composition and nano-size effects that destabilize bonding compete with surface energy as a function of surface composition to dictate particle surface composition. Despite the seemingly minor increase in particle size from 2–5 nm to 4–8 nm after 12 hrs annealing at 700°C, results suggest that the IMCs are significantly stabilized, which may also help energetically drive an adjustment to bulk-like surface composition. Prior catalytic studies also illustrated the increase in Ni+Ga IMC nanoparticle stability after annealing, as evidenced by phase purity being retained even after contacting gas phase reaction conditions of direct ethane and propane dehydrogenation and propane wet reforming up to 600°C with very minor particle size increase after 35 to 82 hrs.^{28,30,32}

In the case of less stable IMC compositions that contain elements that exhibit markedly low surface energy in pure form, e.g., Ni₂In₃, the freeze-annealing conditions used clearly cannot readjust IMC particle surface composition and alternate etching or preparation approaches may be required.^{16,68,169} These results agree with calculated surface energies of a pure In surface vs. a bulk-like terminated Ni₂In₃(110) surface where the former is lower in energy.¹⁶⁹

Another possible approach to control IMC particle surface composition would be to utilize specific gas phase environments that contain specific molecules that bind more strongly to one of the constituent elements of the IMC.¹⁵⁶ For example, utilizing an olefin or CO in combination with H₂ during the initial reduction or annealing procedure may selectively promote higher concentrations of the TM element at the IMC particle surface. This approach was successful for Arenz and co-workers in the manipulation of the surface composition of Pt₃Co where a mixed PtCo_x surface composition could be modified to Pt-rich by using CO during annealing procedures.^{156,170} Likewise, the study of Fe-Cr alloys by Park and co-workers indicated that increased H₂ concentration of annealing atmosphere modified surfaces from Fe-rich to Cr-rich due to the more significant H-Cr interaction.¹⁷⁰ Summarizing, we were able to achieve particle growth and bulk-like surface composition of a selection of IMCs using a freeze-anneal procedure that employed low concentrations of H₂ ultimately achieving well-defined model-like materials.

4 Conclusion

This study developed a fundamental understanding of the synthesis of well-defined supported IMC nanoparticles with pure bulk phase and controllable surface compositions. The understanding can be applied to the entire field of synthesis of well-defined IMCs and enable fundamental structure-activity correlation studies in the fields of heterogeneous catalysis, sensing, and electronics. The fundamental phenomena determined to dictate the forma-

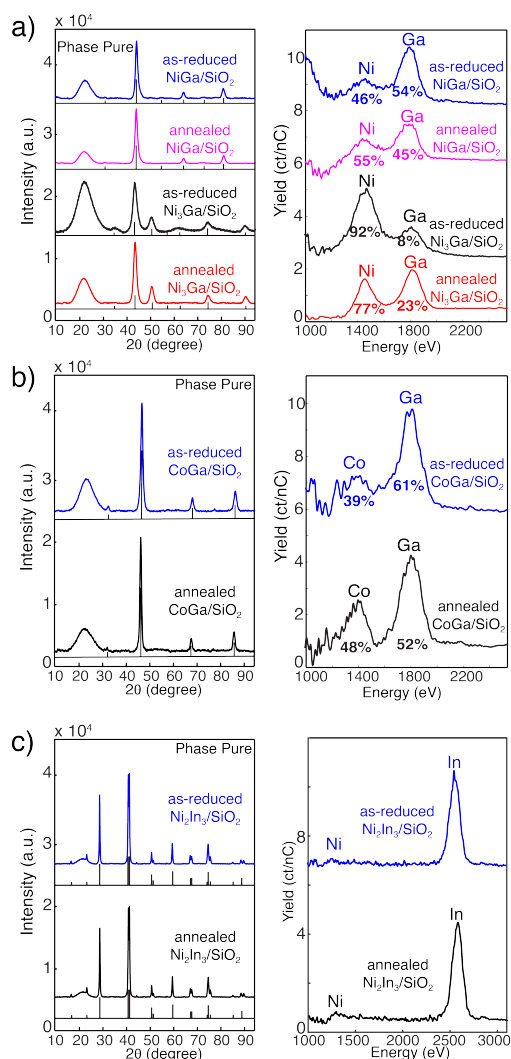


Fig. 9 Demonstration of well-defined IMCs with phase pure bulk and controllable particle surface composition. Long-acquisition-time pXRD and HS-LEIS characterization of: a) as-reduced and freeze-annealed NiGa/SiO₂, and as-reduced and direct-annealed Ni₃Ga/SiO₂; b) as-reduced and freeze-annealed CoGa/SiO₂; and c) as-reduced and freeze-annealed Ni₂In₃/SiO₂.

tion of well-defined supported IMC nanoparticles were: i) reduction kinetics of inorganic salt precursors, ii) formation kinetics of IMC as a function of the diffusion of constituent elements on the surface, iii) the role of support surface chemistry, iv) innate IMC phase stability, and v) the effect of H₂ chemical potential of the reducing and annealing environment. The understanding developed herein can be applied and extended to the entire TM+p-element IMC compositional space with the understanding that the availability of reduced constituent elements and their diffusion across the support will be significant factors when using earlier TMs or more reactive p-elements. Careful choice of precursors and supports with low reactivity will be necessary to realize the synthesis of the entire IMC compositional space as supported nanoparticles.

Conflicts of interest

There are no conflicts to declare.

Acknowledgements

This research was supported by the National Science Foundation (NSF) CAREER award (Grant CBET-1752063) and the American Chemical Society Petroleum Research Fund (Grant PRF# 57589-ND5). Regular XRD analysis were conducted at the Center for Nanophase Materials Sciences (CNMS project number CNMS2018-374) at Oak Ridge National Lab (ORNL). This work utilized the Advanced Photon Source for HR-XRD analysis at Argonne National Laboratory supported by the U. S. Department of Energy, Office of Science, Office of Basic Energy Sciences, under Contract No. DE-AC02-06CH11357.

Notes and references

- 1 C. Breinlich, J. Haubrich, C. Becker, A. Valcarcel, F. Delbecq and K. Wandelt, *J. Catal.*, 2007, **251**, 123–130.
- 2 A. Onda, T. Komatsu and T. Yashima, *Phys. Chem. Chem. Phys.*, 2000, **2**, 2999–3005.
- 3 F. Studt, I. Sharafutdinov, F. Abild-Pedersen, C. F. Elkjær, J. S. Hummelshøj, S. Dahl, I. Chorkendorff and J. K. Nørskov, *Nat. Chem.*, 2014, **6**, 320–324.
- 4 H. Zhao and B. E. Koel, *Surf. Sci.*, 2004, **572**, 261–268.
- 5 I. Sharafutdinov, C. F. Elkjær, H. W. Pereira de Carvalho, D. Gardini, G. L. Chiarello, C. D. Damsgaard, J. B. Wagner, J.-D. Grunwaldt, S. Dahl and I. Chorkendorff, *J. Catal.*, 2014, **320**, 77–88.
- 6 L. Zhang, L. Xue, B. Lin, Q. Zhao, S. Wan, Y. Wang, H. Jia and H. Xiong, *ChemSusChem*, 2022.
- 7 J. Zhang, L. Wang, Y. Shao, Y. Wang, B. C. Gates and F. Xiao, *Angewandte Chemie International Edition*, 2017, **56**, 9747–9751.
- 8 N. Tahsini, A.-C. Yang, V. Streibel, B. Werghe, E. D. Goodman, A. Aitbekova, S. R. Bare, Y. Li, F. Abild-Pedersen and M. Cargnello, *Journal of the American Chemical Society*, 2022, **144**, 1612–1621.
- 9 S. W. Chee, J. M. Arce-Ramos, W. Li, A. Genest and U. Mirsaidov, *Nature Communications*, 2020, **11**, year.
- 10 M. A. van Spronsen, J. W. M. Frenken and I. M. N. Groot, *Chemical Society Reviews*, 2017, **46**, 4347–4374.
- 11 J. Gustafson, O. Balmes, C. Zhang, M. Shipilin, A. Schaefer, B. Hagman, L. R. Merte, N. M. Martin, P.-A. Carlsson, M. Jankowski, E. J. Crumlin and E. Lundgren, *ACS Catalysis*, 2018, **8**, 4438–4445.
- 12 X. Su, P. S. Cremer, Y. R. Shen and G. A. Somorjai, *Journal of the American Chemical Society*, 1997, **119**, 3994–4000.
- 13 T.-H. Yang, J. Ahn, S. Shi, P. Wang, R. Gao and D. Qin, *Chemical Reviews*, 2020, **121**, 796–833.
- 14 A. BORGSCHULTE, R. WESTERWAAL, J. RECTOR, H. SCHREUDERS, B. DAM and R. GRIESSEN, *Journal of Catalysis*, 2006, **239**, 263–271.
- 15 L. E. Murillo, C. A. Menning and J. G. Chen, *J. Catal.*, 2009, **268**, 335–342.

- 16 H.-Y. Park, T.-Y. Jeon, J. H. Jang, S. J. Yoo, K.-H. Choi, N. Jung, Y.-H. Chung, M. Ahn, Y.-H. Cho, K.-S. Lee and et al., *Applied Catalysis B: Environmental*, 2013, **129**, 375–381.
- 17 A. Bruix, Y. Lykhach, I. Matolínová, A. Neitzel, T. Skála, N. Tsud, M. Vorokhta, V. Stetsovych, K. Ševčíková, J. Mysliveček, R. Fiala, M. Václavů, K. C. Prince, S. Bruyère, V. Potin, F. Illas, V. Matolín, J. Libuda and K. M. Neyman, *Angewandte Chemie International Edition*, 2014, **53**, 10525–10530.
- 18 F. Studt, F. Abild-Pedersen, T. Bligaard, R. Z. Sorensen, C. H. Christensen and J. K. Norskov, *Science*, 2008, **320**, 1320–1322.
- 19 L. Rößner and M. Armbrüster, *ACS Catal.*, 2019, **9**, 2018–2062.
- 20 E. W. Shin, C. H. Choi, K. S. Chang, Y. H. Na and S. H. Moon, *Catal. Today*, 1998, **44**, 137–143.
- 21 M. Armbrüster, K. Kovnir, M. Behrens, D. Teschner, Y. Grin and R. Schlögl, *J. Am. Chem. Soc.*, 2010, **132**, 14745–14747.
- 22 H. Zhao, J. Kim and B. E. Koel, *Surf. Sci.*, 2003, **538**, 147–159.
- 23 B. Riguetto, C. Rodrigues, M. Morales, E. Baggio-Saitovitch, L. Gengembre, E. Payen, C. Marques and J. Bueno, *Applied Catalysis A: General*, 2007, **318**, 70–78.
- 24 H. Göksu, S. F. Ho, Ö. Metin, K. Korkmaz, A. Mendoza Garcia, M. S. Gültekin and S. Sun, *ACS Catal.*, 2014, **4**, 1777–1782.
- 25 K. Tomishige, K. Asakura and Y. Iwasawa, *J. Catal.*, 1994, **149**, 70–80.
- 26 Y. He and S. Laursen, *ACS Catal.*, 2017, **7**, 3169–3180.
- 27 Y. He and S. Laursen, *Catal. Sci. Technol.*, 2018, **8**, 5302–5314.
- 28 Y. He, Y. Song, D. A. Cullen and S. Laursen, *J. Am. Chem. Soc.*, 2018, **140**, 14010–14014.
- 29 Y. He and S. Laursen, *Surf. Sci.*, 2019, **686**, 1–9.
- 30 Y. He, Y. Song and S. Laursen, *ACS Catal.*, 2019, **9**, 10464–10468.
- 31 Y. Song and S. Laursen, *J. Catal.*, 2019, **372**, 151–162.
- 32 Y. Song, Y. He and S. Laursen, *ACS Catal.*, 2020, **10**, 8968–8980.
- 33 S. Poudyal and S. Laursen, *The Journal of Physical Chemistry C*, 2018, **122**, 8045–8057.
- 34 S. Poudyal and S. Laursen, *Catal. Sci. Technol.*, 2019, **9**, 1048–1059.
- 35 S. Poudyal, M. Parker and S. Laursen, *The Journal of Physical Chemistry Letters*, 2019, **10**, 4603–4608.
- 36 J. K. Nørskov, F. Abild-Pedersen, F. Studt and T. Bligaard, *Proceedings of the National Academy of Sciences*, 2011, **108**, 937–943.
- 37 J. Chen, *J. Catal.*, 1995, **154**, 80–90.
- 38 J. G. Chen, M. D. Weisel, Z. M. Liu and J. M. White, *J. Am. Chem. Soc.*, 1993, **115**, 8875–8876.
- 39 H. Ren, Y. Chen, Y. Huang, W. Deng, D. G. Vlachos and J. G. Chen, *Green Chem.*, 2014, **16**, 761–769.
- 40 J. Chen and B. Fruhberger, *Surf. Sci.*, 1996, **367**, L102–L110.
- 41 B. M. Wyvrat, J. R. Gaudet, D. B. Pardue, A. Marton, S. Rudić, E. A. Mader, T. R. Cundari, J. M. Mayer and L. T. Thompson, *ACS Catal.*, 2016, **6**, 5797–5806.
- 42 M. Neylon, S. Choi, H. Kwon, K. Curry and L. Thompson, *Applied Catalysis A: General*, 1999, **183**, 253–263.
- 43 M. D. Porosoff, S. Kattel, W. Li, P. Liu and J. G. Chen, *Chemical Communications*, 2015, **51**, 6988–6991.
- 44 J. Giner, *J. Catal.*, 1967, **9**, 115–124.
- 45 S. Kishida, *J. Catal.*, 1968, **12**, 97–101.
- 46 M. Masai, *J. Catal.*, 1975, **38**, 128–134.
- 47 C. Xu and B. E. Koel, *Surf. Sci.*, 1994, **304**, 249–266.
- 48 P. Forzatti, *J. Catal.*, 1982, **76**, 188–207.
- 49 Y. Nitta, T. Imanaka and S. Teranishi, *Bull. Chem. Soc. Jpn.*, 1981, **54**, 3579–3580.
- 50 J. A. Schreifels, P. C. Maybury and W. E. Swartz, *The Journal of Organic Chemistry*, 1981, **46**, 1263–1269.
- 51 H. Aduriz, *J. Catal.*, 1989, **119**, 97–107.
- 52 G. Hamm, T. Schmidt, J. Breitbach, D. Franke, C. Becker and K. Wandelt, *Surf. Sci.*, 2004, **562**, 170–182.
- 53 D. I. Jerdev, A. Olivas and B. E. Koel, *J. Catal.*, 2002, **205**, 278–288.
- 54 R. Rodiansono, M. D. Astuti, S. Khairi and S. Shimazu, *Bull. Chem. React. Eng. Catal.*, 2016, **11**, 1.
- 55 C. Li, Y. Chen, S. Zhang, J. Zhou, F. Wang, S. He, M. Wei, D. Evans and X. Duan, *ChemCatChem*, 2014, **6**, 824–831.
- 56 J. Gao, H. Zhao, X. Yang, B. E. Koel and S. G. Podkolzin, *ACS Catal.*, 2013, **3**, 1149–1153.
- 57 Q. Feng, S. Zhao, Y. Wang, J. Dong, W. Chen, D. He, D. Wang, J. Yang, Y. Zhu, H. Zhu and et al., *J. Am. Chem. Soc.*, 2017, **139**, 7294–7301.
- 58 K. Kovnir, J. Osswald, M. Armbruster, D. Teschner, G. W. U. Wild, A. Knop-Gericke, T. Ressler, Y. Grin and R. Schlögl, *J. Catal.*, 2009, **264**, 93–103.
- 59 T. Komatsu, T. Kishi and T. Gorai, *J. Catal.*, 2008, **259**, 174–182.
- 60 Y. Chen and J. Chen, *Appl. Surf. Sci.*, 2016, **387**, 16–27.
- 61 J. Shabaker, D. Simonetti, R. Cortright and J. Dumesic, *J. Catal.*, 2005, **231**, 67–76.
- 62 A. García-Trenco, A. Regoutz, E. R. White, D. J. Payne, M. S. Shaffer and C. K. Williams, *Applied Catalysis B: Environmental*, 2018, **220**, 9–18.
- 63 T. Komatsu, M. Mesuda and T. Yashima, *Applied Catalysis A: General*, 2000, **194-195**, 333–339.
- 64 S. Penner and P. D. Kheyrollahi Nezhad, *ACS Catalysis*, 2021, **11**, 5271–5286.
- 65 L. Xiao, P. Hu, Z.-J. Sui, D. Chen, X.-G. Zhou, W.-K. Yuan and Y.-A. Zhu, *Journal of Catalysis*, 2021, **404**, 32–45.
- 66 M. G. Kanatzidis, R. Pöttgen and W. Jeitschko, *Angewandte Chemie International Edition*, 2005, **44**, 6996–7023.
- 67 A. Onda, T. Komatsu and T. Yashima, *J. Catal.*, 2004, **221**, 378–385.
- 68 J. Osswald, R. Giedigkeit, R. Jentoft, M. Armbruster, F. Girgsdies, K. Kovnir, T. Ressler, Y. Grin and R. Schlögl, *J. Catal.*,

- 2008, **258**, 210–218.
- 69 M. Fan, Y. Xu, J. Sakurai, M. Demura, T. Hirano, Y. Teraoka and A. Yoshigoe, *Int. J. Hydrogen Energy*, 2015, **40**, 12663–12673.
- 70 C. Yeh and C. Yeh, *J. Alloys Compd.*, 2005, **388**, 241–249.
- 71 C. Milanese, F. Maglia, A. Tacca, U. Anselmi-Tamburini, C. Zanotti and P. Giuliani, *J. Alloys Compd.*, 2006, **421**, 156–162.
- 72 S. Meschel, P. Nash and X.-Q. Chen, *J. Alloys Compd.*, 2010, **492**, 105–115.
- 73 V. Gauthier, F. Bernard, E. Gaffet, D. Vrel, M. Gailhanou and J. Larpin, *Intermetallics*, 2002, **10**, 377–389.
- 74 H. Yoshida, T. Shima, T. Takahashi and H. Fujimori, *Mater. Trans., JIM*, 1999, **40**, 455–458.
- 75 T. Chanadee, J. Wannasin and S. Niyomwas, *J. Ceram. Soc. Jpn.*, 2014, **122**, 496–501.
- 76 L. A. Arkatova, L. N. Kurina and L. V. Galaktionova, *Russ. J. Phys. Chem. A*, 2009, **83**, 624–629.
- 77 N. Köwitsch, S. Barth, K. Ploner, R. Blume, D. Teschner, S. Penner and M. Armbrüster, *ChemPhysChem*, 2022.
- 78 G. Wowsnick, D. Teschner, M. Armbrüster, I. Kasatkin, F. Girgsdies, Y. Grin, R. Schlögl and M. Behrens, *J. Catal.*, 2014, **309**, 221–230.
- 79 G. Wowsnick, D. Teschner, I. Kasatkin, F. Girgsdies, M. Armbrüster, A. Zhang, Y. Grin, R. Schlögl and M. Behrens, *J. Catal.*, 2014, **309**, 209–220.
- 80 S. Zafeiratos, S. Piccinin and D. Teschner, *Catal. Sci. Technol.*, 2012, **2**, 1787.
- 81 L. Zhen, Y. X. Gong, J. T. Jiang and W. Z. Shao, *Journal of Applied Physics*, 2008, **104**, 034312.
- 82 Z. Cui, H. Chen, M. Zhao and F. J. DiSalvo, *Nano Lett.*, 2016, **16**, 2560–2566.
- 83 Y.-T. Pan, Y. Yan, Y.-T. Shao, J.-M. Zuo and H. Yang, *Nano Lett.*, 2016, **16**, 6599–6603.
- 84 J.-H. Liu, L.-D. Meng, C.-Q. Lv and G.-C. Wang, *RSC Adv.*, 2016, **6**, 14593–14601.
- 85 J. C. Bauer, X. Chen, Q. Liu, T.-H. Phan and R. E. Schaak, *J. Mater. Chem.*, 2008, **18**, 275–282.
- 86 X. Chen, M. Li, J. Guan, X. Wang, C. T. Williams and C. Liang, *Ind. Eng. Chem. Res.*, 2012, **51**, 3604–3611.
- 87 R. E. Cable and R. E. Schaak, *Chem. Mater.*, 2007, **19**, 4098–4104.
- 88 R. E. Cable and R. E. Schaak, *Chem. Mater.*, 2005, **17**, 6835–6841.
- 89 A. K. Sra and R. E. Schaak, *J. Am. Chem. Soc.*, 2004, **126**, 6667–6672.
- 90 R. E. Schaak, A. K. Sra, B. M. Leonard, R. E. Cable, J. C. Bauer, Y.-F. Han, J. Means, W. Teizer, Y. Vasquez and E. S. Funck, *J. Am. Chem. Soc.*, 2005, **127**, 3506–3515.
- 91 Y. Yuan, Z. Yang, W. Lai, L. Gao, M. Li, J. Zhang and H. Huang, *Chemistry – A European Journal*, 2021, **27**, 16564–16580.
- 92 S. Furukawa, K. Takahashi and T. Komatsu, *Chem. Sci.*, 2016, **7**, 4476–4484.
- 93 L. Sordelli, R. Psaro, G. Vlaic, A. Cepparo, S. Recchia, C. Dossi, A. Fusi and R. Zaroni, *J. Catal.*, 1999, **182**, 186–198.
- 94 C. Li, Y. Chen, S. Zhang, S. Xu, J. Zhou, F. Wang, M. Wei, D. G. Evans and X. Duan, *Chem. Mater.*, 2013, **25**, 3888–3896.
- 95 J. L. Snider, V. Streibel, M. A. Hubert, T. S. Choksi, E. Valle, D. C. Upham, J. Schumann, M. S. Duyar, A. Gallo, F. Abild-Pedersen and J. T. F., *ACS Catal.*, 2019, **9**, 3399–3412.
- 96 S. Furukawa, K. Ozawa and T. Komatsu, *RSC Adv.*, 2013, **3**, 23269.
- 97 L. Li, B. Zhang, E. Kunkes, K. Föttinger, M. Armbrüster, D. S. Su, W. Wei, R. Schlögl and M. Behrens, *ChemCatChem*, 2012, **4**, 1764–1775.
- 98 J. Serrano-Ruiz, A. Sepúlveda-Escribano, F. Rodríguez-Reinoso and D. Duprez, *J. Mol. Catal. A: Chem.*, 2007, **268**, 227–234.
- 99 F. Marchesini, S. Irusta, C. Querini and E. Miró, *Applied Catalysis A: General*, 2008, **348**, 60–70.
- 100 J. Llorca, *J. Catal.*, 1995, **156**, 139–146.
- 101 N. Kaylor, J. Xie, Y.-S. Kim, H. N. Pham, A. K. Datye, Y.-K. Lee and R. J. Davis, *J. Catal.*, 2016, **344**, 202–212.
- 102 J. Zhou, Y. Yang, C. Li, S. Zhang, Y. Chen, S. Shi and M. Wei, *J. Mater. Chem. A*, 2016, **4**, 12825–12832.
- 103 J. Shabaker, G. Huber and J. Dumesic, *J. Catal.*, 2004, **222**, 180–191.
- 104 C. Rudolf, B. Dragoi, A. Ungureanu, A. Chiriac, S. Royer, A. Nastro and E. Dumitriu, *Catal. Sci. Technol.*, 2014, **4**, 179–189.
- 105 Y. Ma, Y. Xu, M. Demura, D. H. Chun, G. Xie and T. Hirano, *Catal. Lett.*, 2006, **112**, 31–36.
- 106 X. Chen, Y. Ma, L. Wang, Z. Yang, S. Jin, L. Zhang and C. Liang, *ChemCatChem*, 2015, **7**, 978–983.
- 107 T. Komatsu, M. Fukui and T. Yashima, *Stud. Surf. Sci. Catal.*, 1996, 1095–1104.
- 108 V. Lockett, R. Sedev, C. Bassell and J. Ralston, *Phys. Chem. Chem. Phys.*, 2008, **10**, 1330.
- 109 R. Steinberger, C. Celedón, B. Bruckner, D. Roth, J. Duchoslav, M. Arndt, P. Kürnsteiner, T. Steck, J. Faderl, C. Riener and et al., *Appl. Surf. Sci.*, 2017, **411**, 189–196.
- 110 K. Cai, M. Müller, J. Bossert, A. Rechtenbach and K. D. Jandt, *Appl. Surf. Sci.*, 2005, **250**, 252–267.
- 111 J. Zheng, J. Qu, H. Lin, Q. Zhang, X. Yuan, Y. Yang and Y. Yuan, *ACS Catal.*, 2016, **6**, 6662–6669.
- 112 F. Polo-Garzon, S.-Z. Yang, V. Fung, G. S. Foo, E. E. Bickel, M. F. Chisholm, D.-e. Jiang and Z. Wu, *Angewandte Chemie International Edition*, 2017, **56**, 9820–9824.
- 113 G. S. Foo, Z. D. Hood and Z. Wu, *ACS Catal.*, 2017, **8**, 555–565.
- 114 M. Lefèvre, J. P. Dodelet and P. Bertrand, *The Journal of Physical Chemistry B*, 2005, **109**, 16718–16724.
- 115 R. N. S. Sodhi, *The Analyst*, 2004, **129**, 483–487.
- 116 D. J. Graham and D. G. Castner, *Biointerphases*, 2012, **7**, 49.

- 117 P. Massonnet and R. M. A. Heeren, *J. Anal. At. Spectrom.*, 2019, **34**, 2217–2228.
- 118 S. P. Phivilay, C. A. Roberts, A. A. Puzos, K. Domen and I. E. Wachs, *The Journal of Physical Chemistry Letters*, 2013, **4**, 3719–3724.
- 119 S. P. Phivilay, C. A. Roberts, A. D. Gamalski, E. A. Stach, S. Zhang, L. Nguyen, Y. Tang, A. Xiong, A. A. Puzos, F. F. Tao and et al., *ACS Catal.*, 2018, **8**, 6650–6658.
- 120 G. S. Foo, F. Polo-Garzon, V. Fung, D.-e. Jiang, S. H. Overbury and Z. Wu, *ACS Catal.*, 2017, **7**, 4423–4434.
- 121 G. M. Rupp, H. Téllez, J. Druce, A. Limbeck, T. Ishihara, J. Kilner and J. Fleig, *J. Mater. Chem. A*, 2015, **3**, 22759–22769.
- 122 X. Li, D. Li, H. Tian, L. Zeng, Z.-J. Zhao and J. Gong, *Applied Catalysis B: Environmental*, 2017, **202**, 683–694.
- 123 J. Druce, H. Téllez, M. Burriel, M. D. Sharp, L. J. Fawcett, S. N. Cook, D. S. McPhail, T. Ishihara, H. H. Brongersma and J. A. Kilner, *Energy Environ. Sci.*, 2014, **7**, 3593–3599.
- 124 X. LI, W. JI, J. ZHAO, S. WANG and C. AU, *Journal of Catalysis*, 2005, **236**, 181–189.
- 125 L. Wang, Y. Yi, Y. Zhao, R. Zhang, J. Zhang and H. Guo, *ACS Catalysis*, 2015, **5**, 4167–4174.
- 126 Z. Lu, G. Chen, S. Siahrostami, Z. Chen, K. Liu, J. Xie, L. Liao, T. Wu, D. Lin, Y. Liu, T. F. Jaramillo, J. K. Nørskov and Y. Cui, *Nature Catalysis*, 2018, **1**, 156–162.
- 127 J. H. Kim, J. Y. Cheon, T. J. Shin, J. Y. Park and S. H. Joo, *Carbon*, 2016, **101**, 449–457.
- 128 D. J. Suh, P. Tae-Jin and I. Son-Ki, *Carbon*, 1993, **31**, 427–435.
- 129 E. Plessers, J. E. vandenReijen, P. E. deJongh, K. P. deJong and M. B. J. Roelofs, *ChemCatChem*, 2017, **9**, 4562–4569.
- 130 W. Juszczak, Z. Karpinski, D. Lomot, J. Pielaszek, Z. Paal and A. Stakheev, *Journal of Catalysis*, 1993, **142**, 617–629.
- 131 S. Wang and G. Lu, *Applied Catalysis A: General*, 1998, **169**, 271–280.
- 132 E. Kowalewski, I. I. Kamińska, G. Słowik, D. Lisovtshiy and A. Śrębowata, *React. Kin., Mech. Catal.*, 2017, **121**, 3–16.
- 133 S. Laursen and S. Linic, *The Journal of Physical Chemistry C*, 2009, **113**, 6689–6693.
- 134 S. Laursen and S. Linic, *Phys. Chem. Chem. Phys.*, 2009, **11**, 11006.
- 135 X. Wen, R. Li, Y. Yang, J. Chen and F. Zhang, *Applied Catalysis A: General*, 2013, **468**, 204–215.
- 136 Y. Huang, X. Chen, Y. Deng, D. Zhou and L. Wang, *Chemical Engineering Journal*, 2015, **269**, 434–443.
- 137 M. A. Ermakova and D. Y. Ermakov, *Applied Catalysis A: General*, 2003, **245**, 277–288.
- 138 E. v. Steen, G. S. Sewell, R. A. Makhothe, C. Micklethwaite, H. Manstein, M. de Lange and C. T. O'Connor, *Journal of Catalysis*, 1996, **162**, 220–229.
- 139 H. Kusaka, Y. Hara, M. Onuki, T. Akai and M. Okuda, *Journal of Catalysis*, 1996, **161**, 96–106.
- 140 D. Eliche-Quesada, J. Mérida-Robles, E. Rodríguez-Castellón and A. Jiménez-López, *Applied Catalysis A: General*, 2005, **279**, 209–221.
- 141 W. C. Conner and J. L. Falconer, *Chemical Reviews*, 1995, **95**, 759–788.
- 142 B. Sen, *J. Catal.*, 1989, **117**, 404–415.
- 143 P. Kim, H. Kim, J. B. Joo, W. Kim, I. K. Song and J. Yi, *J. Mol. Catal. A: Chem.*, 2006, **256**, 178–183.
- 144 G. Wu, C. Zhang, S. Li, Z. Han, T. Wang, X. Ma and J. Gong, *ACS Sustainable Chem. Eng.*, 2013, **1**, 1052–1062.
- 145 N. Keghouche, S. Chettibi, F. Latrèche, M. Bettahar, J. Belloni and J. Marignier, *Radiat. Phys. Chem.*, 2005, **74**, 185–200.
- 146 W. W. Rudolph, D. Fischer, M. R. Tomney and C. C. Pye, *Phys. Chem. Chem. Phys.*, 2004, **6**, 5145–5155.
- 147 F. Maglia, U. Anselmi-Tamburini, N. Bertolino, C. Milanese and Z. A. Munir, *J. Mater. Res.*, 2001, **16**, 534–544.
- 148 H. Okamoto, *J. Phase Equilib. Diffus.*, 2008, **29**, 296–296.
- 149 P. Durussel, G. Burri and P. Feschotte, *J. Alloys Compd.*, 1997, **257**, 253–258.
- 150 L. Wang, X. Niu and J. Chen, *Applied Catalysis B: Environmental*, 2020, **278**, 119293.
- 151 T. Komatsu, *Applied Catalysis A: General*, 2003, **251**, 315–326.
- 152 A. P. Tsai, S. Kameoka, K. Nozawa, M. Shimoda and Y. Ishii, *Acc. Chem. Res.*, 2017, **50**, 2879–2885.
- 153 A. K. Vivekanandan, B. Muthukutty, S.-M. Chen, M. Sivakumar and S.-H. Chen, *ACS Sustainable Chem. Eng.*, 2020, **8**, 17718–17726.
- 154 Y. Satake, K. Fujiwara, J. Shiogai, T. Seki and A. Tsukazaki, *Sci. Rep.*, 2019, **9**, year.
- 155 Z. Fang, S. Duan, H. Liu, Z. Hong, H. Wu, F. Zhao, Q. Li, S. Fan, W. Duan and J. Wang, *Small*, 2021, **18**, 2105172.
- 156 K. Mayrhofer, V. Juhart, K. Hartl, M. Hanzlik and M. Arenz, *Angewandte Chemie International Edition*, 2009, **48**, 3529–3531.
- 157 M. Friedrich, D. Teschner, A. Knop-Gericke and M. Armbrüster, *J. Catal.*, 2012, **285**, 41–47.
- 158 B. Zugic, L. Wang, C. Heine, D. N. Zakharov, B. A. J. Lechner, E. A. Stach, J. Biener, M. Salmeron, R. J. Madix and C. M. Friend, *Nat. Mater.*, 2016, **16**, 558–564.
- 159 M. Krajčí and J. Hafner, *Phys. Rev. B*, 2013, **87**, year.
- 160 E. Antolini, *Applied Catalysis B: Environmental*, 2017, **217**, 201–213.
- 161 S. Furukawa and T. Komatsu, *ACS Catal.*, 2016, **7**, 735–765.
- 162 P. Dantzer, *Materials Science and Engineering: A*, 2002, **329-331**, 313–320.
- 163 H. Orita, *Journal of Catalysis*, 1984, **90**, 183–193.
- 164 C. C. Tang, S. S. Fan, H. Y. Dang, P. Li and Y. M. Liu, *Applied Physics Letters*, 2000, **77**, 1961–1963.
- 165 P. Burattin, M. Che and C. Louis, *The Journal of Physical Chemistry B*, 1999, **103**, 6171–6178.
- 166 W. Józwiak, M. Nowosielska and J. Rynkowski, *Applied Catalysis A: General*, 2005, **280**, 233–244.
- 167 Y. K. Kim, D. A. Baugh, D. K. Shuh, R. Stanley Williams, L. P. Sadwick and K. L. Wang, *J. Mater. Res.*, 1990, **5**, 2139–2151.

- 168 D. Rosenthal, R. Widmer, R. Wagner, P. Gille, M. Armbrüster, Y. Grin, R. Schlögl and O. Gröning, *Langmuir*, 2012, **28**, 6848–6856.
- 169 L. Vitos, A. Ruban, H. Skriver and J. Kollár, *Surf. Sci.*, 1998, **411**, 186–202.
- 170 E. Park, B. Hünig and M. Spiegel, *Appl. Surf. Sci.*, 2005, **249**, 127–138.